Bulgarian Chemical Communications, Volume 51, Special Issue D (pp. 158 – 164) 2019

Catalytic activation of PMS by Co_3O_4 modified *g*-C_3N_4 for oxidative degradation of the azo dye Acid Orange 7 in aqueous solutions

V. V. Ivanova-Kolcheva, M. K. Stoyanova*

Department of Physical Chemistry, University of Plovdiv, 24 Tzar Assen Str, Plovdiv, 4000, Bulgaria

Received November 14, 2018; Revised January 16, 2019

Co_3O_4 modified g-C_3N_4 catalysts were prepared by a facile one-pot thermal polycondensation method using pure and HNO_3 protonated melamine as graphitic carbon nitride precursors. The materials were thoroughly characterized by a variety of techniques including XRD, TEM, BET, ICP-OES, and FT-IR-spectroscopy and their catalytic activity for degradation of the model azo dye Acid Orange 7 (AO7) in aqueous solutions based on the activation of peroxymonosulfate (PMS) without light irradiation was evaluated. The prepared composite catalysts demonstrated to be much more efficient in activating PMS for AO7 degradation than pure Co_3O_4. The Co-g-C_3N_4 (pm) hybrid exhibited better catalytic activity (k=0.1391 min^{-1}) than the catalyst prepared by sintering melamine without protonation (k=0.0646 min^{-1}). The enhanced catalytic performance of the Co-g-C_3N_4 (pm) could be attributed to the larger specific surface area, supplying more surface active sites and to the higher condensation degree of the g-C_3N_4. The degradation of AO7 was found to follow the first order kinetics. The effect of catalyst dosage, PMS concentration and pH on the rate of AO7 degradation was investigated. The radical species generated from the catalytic decomposition of PMS were identified by quenching studies.

Keywords: graphitic carbon nitride, Co_3O_4, peroxymonosulfate, catalytic degradation, Acid Orange 7

INTRODUCTION

The uncontrolled disposal of refractory organic contaminants in aquatic systems is an essential environmental issue, as pollutants could not only be accumulated in the various components of the environment but by migration, they can fall into the food chains and can induce severe public health problems. A considerable source of water pollution is the discharge of dye effluents by various industries (e.g. textile, pulp and paper, leather, food, dyestuff manufacturing, etc.). It is estimated that approximately 15% of the textile dyes produced are lost in the industrial effluents during manufacturing or processing operations [1]. In the recent years, advanced oxidation processes based on peroxymonosulfate (PMS) activation for generating sulfate radicals (SRs) is extensively investigated as an effective and eco-friendly technology for degrading organic pollutants in water [2,3]. Compared to the conventional Fenton process, SRs generating processes have a number of advantages because sulfate radicals have similar or even higher oxidation potential than hydroxyl radicals, are effective over a wide range of pH (pH 2–9), have a significantly longer lifetime (30–40 μs *vs* 20 ns), and exhibit a much higher selectivity in the presence of complex environmental matrices [4, 5].

The most commonly used PMS activators are transition metals-based catalysts (Co, Mn, Cu, Fe) used both in homogeneous and heterogeneous systems [6, 7]. Homogeneous catalytic activation of PMS by transition metal ions is proven to be the most efficient route for quick production of SRs at room temperature, with cobalt ions being indentified as the most efficient PMS activator [1]. However, this process causes secondary pollutions and requires recovering the homogeneous catalyst from the treated water that is not often technically or economically feasible. Therefore, the heterogeneous catalysts are preferred for PMS activation. Various transition metal oxides and their combinations have been used to activate PMS, such as Co_3O_4, Mn_3O_2, $CuFe_2O_4$, Fe_3O_4, CuO, $CoFe_2O_4$, etc. [6, 7]. Due to the highest efficiency of cobalt-containing catalysts for generating SRs by PMS decomposition, the Co_3O_4/PMS system has been thoroughly investigated for organic pollutants degradation [8]. Despite the excellent performance of Co_3O_4 nanoparticles in PMS activation, they easily agglomerate, resulting in a decrease in catalytic effectiveness [9]. In order to improve the catalytic activity and stability of Co_3O_4, it was immobilized on different supports such as MgO, TiO_2, SiO_2, activated carbon, graphene, zeolite, etc. [10, 11]. Recently, the photocatalytic activation of PMS using environmentally friendly nonmetal carbon-based catalysts as activated carbon, graphene oxide, and carbon nanotubes is of

* To whom all correspondence should be sent.
E-mail: marianas@uni-plovdiv.bg

increasing interest. It was found that nitrogen doping on carbon catalysts boosted their catalytic activity for PMS decomposition [12, 13]. Although graphitic-carbon nitride (g-C_3N_4) is a nitrogen-rich material, its sole use for PMS activation was ineffective even under visible light irradiation [14]. Modifying g-C_3N_4 with iron oxide and cobalt oxide leads to enhanced photocatalytic activity toward organics degradation [15, 16]. So far there are no published data on the activation of PMS by g-C_3N_4 modified with transition metal oxides at ambient conditions.

The aim of the present study is to evaluate the PMS activation performance of Co_3O_4 modified g-C_3N_4 prepared from protonated melamine for oxidative degradation of AO7 dye in aqueous solution without light irradiation.

EXPERIMENTAL

Pristine g-C_3N_4 (represented as g-C_3N_4 (pm)) was prepared by thermal condensation of protonated melamine according to the procedure, described in [17]. In brief, 12 g od melamine was dissolved into 100 cm^3 of methanol (MeOH) at 60ºC and stirred for 10 min. Then, a certain amount of 0.2 M HNO_3 was added dropwise into the above solution. The obtained white precipitate was separated out, washed several times with MeOH, dried at 60 ºC for 10 h, and finally calcined at 550 ºC for 2 h in static air. Co-g-C_3N_4 (pm) composite was prepared by a one-pot synthetic approach. A certain amount of $Co(NO_3)_2 \cdot 6H_2O$ to reach 5 wt.% Co in the final catalyst was dissolved in 50 cm^3 of MeOH and added to the desired amount of protonated melamine under continuous stirring. The suspension was stirred at 50 ºC until MeOH was evaporated, then the obtained solid was dried at 60 ºC for 10 h and calcined at 550 ºC for 2 h. For comparison, pristine and Co_3O_4 modified g-C_3N_4 were prepared following the procedure mentioned above using melamine without protonation with HNO_3.

The amount of cobalt in the prepared catalysts was measured by ICP-OES analysis (iCAP 6300 Thermo Scientific). XRD patterns of the samples were obtained on a TUR-MA 62 powder diffractometer, using Co-Kα radiation (λ= 1.789 Å) at 40 kV and 20 mA. The morphology of the samples was characterized by a JEOL JEM 2100 high resolution transmission electron microscope (TEM) using an accelerating voltage of 200 kV. The BET specific surface area was determined using a Micromeritics apparatus (Tristar 3000 porosimeter). Infrared spectra were recorded with a Fourier transform infrared spectrometer (Vertex 70, Bruker Optics).

The degradation of AO7 was carried out at room temperature (20±2◦C) in 400 cm^3 batch reactor with constant stirring at 400 rpm. In a typical run, a fixed amount of PMS (in the form of Oxone, $2KHSO_5.KHSO_4.K_2SO_4$) was added to 200 cm^3 of 50 mg dm^{-3} AO7 aqueous solution to achieve the predefined PMS/AO7 molar ratio and was stirred until dissolved. Degradation reaction was initiated by the addition of a specified amount of catalyst. Aliquots of 4.0 cm^3 were taken at given time intervals, quenched immediately by adding 1 cm^3 of methanol, and centrifuged at 4000 rpm for 1 min to remove the catalyst. The AO7 concentration in the filtrate was determined by UV–Vis spectroscopy (Cintra 101, GBS) at 486 nm. All experiments were conducted in triplicate.

RESULTS AND DISCUSSION

The cobalt weight percentage in the final composite catalysts as determined by ICP-OES was found to be close to preparation settings, corresponding to 5 wt% .

Fig. 1 displays the XRD patterns of the pristine g-C_3N_4 (pm) and Co-doped g-C_3N_4 (pm) catalysts. The pure g-C_3N_4 (pm) shows two distinct diffraction peaks at 2Θ =15.2° and 32.2° (higher intensity), which confirms its graphitic-like layer structure. The strongest peak indexed for (002) diffraction planes in g-C_3N_4 (pm) reveals graphitic stacking of C_3N_4 layers. A relatively weak peak at 15.2° can be attributed to an in-planar ordering of tri-s-triazine units, which was indexed as (100). The Co-g-C_3N_4 (pm) catalyst shows similar XRD patterns with no shifting in the two characteristic g-C_3N_4 (pm) peaks. However, the intensity of (002) peak decreases and also broadens in case of the doped sample, which indicates that Co_3O_4 species restrain the growth of crystal structure of g-C_3N_4. Diffraction peaks of Co_3O_4 species are not observed in the patterns of Co-g-C_3N_4 (pm) catalyst, which could be attributed to the low Co content (5 wt%) as well as to the very small grain size effects, thus not detected by this technique.

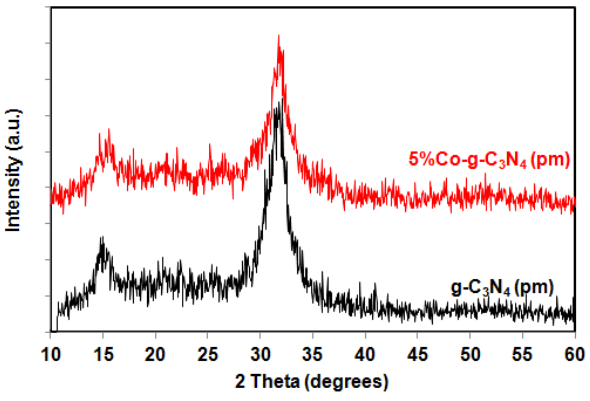

Figure 1. XRD patterns of pristine and Co_3O_4 modified *g*-C_3N_4 (pm)

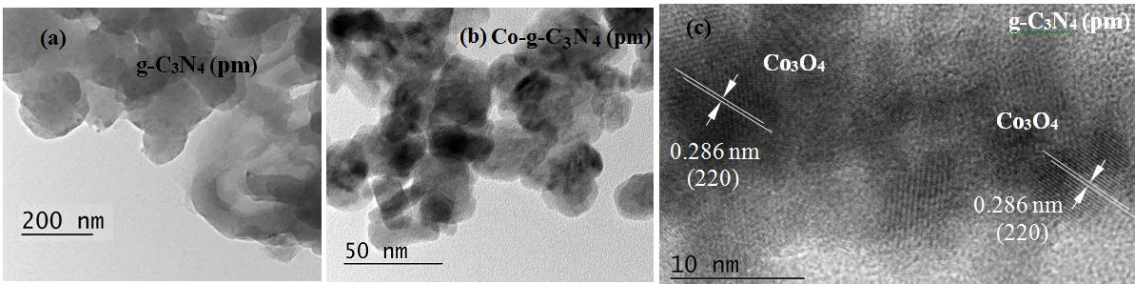

Figure 2. TEM images of (a) *g*-C_3N_4 (pm) and (b, c) Co-*g*-C_3N_4 (pm)

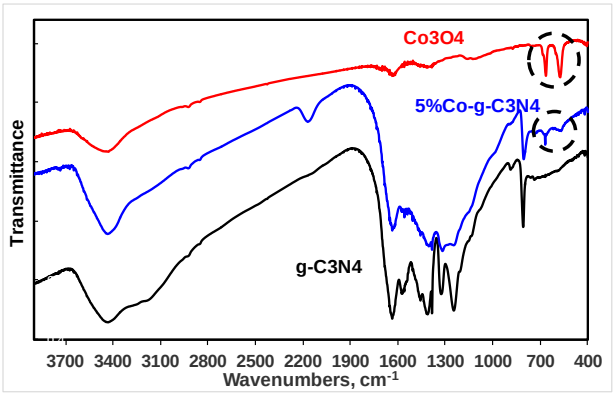

Figure 3. FTIR spectra of synthesized catalysts

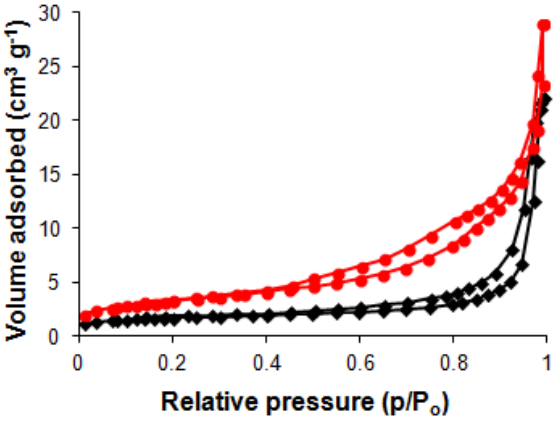

Figure 4. N_2 adsorption/desorption isotherms of g-C_3N_4 (pm) and Co-g-C_3N_4 (pm)

The bright field TEM images of g-C_3N_4 (pm) and Co-g-C_3N_4 (pm) are presented in Fig. 2. Pristine g-C_3N_4 (pm) sample shows a typical layer structure with planar aggregates of g-C_3N_4 sheets as observed in Fig. 2a. For Co-g-C_3N_4 (pm) catalyst, Co_3O_4 species (dark spots in Fig. 2b) with close to the spherical shape and sizes ranging from 10 to 25 nm are distributed throughout the sheets of g-C_3N_4 particles. Although not detectable by the XRD technique, Fig. 2c confirms the presence of catalytically active Co_3O_4 phase in the Co-g-C_3N_4 (pm) hybrid. The HRTEM image shows well-defined lattice fringes with d-spacing value of 0.286 nm, which can be assigned to (220) plane of Co_3O_4 cubic spinel phase.

The graphitic structures of the as-prepared samples were further demonstrated by FTIR spectra. Fig. 3 compares FTIR spectra of pristine g-C_3N_4 (pm), pure Co_3O_4 and Co-g-C_3N_4 (pm) taken in transmittance mode between 400 and 4000 cm^{-1}. It can be clearly observed that the features of the condensed C–N heterocycles are present in the spectra of both pure and Co_3O_4 doped graphitic carbon nitride. For these samples, the sharp peak located at about 809 cm^{-1} can be assigned to the out-of-plane bending vibration mode of tri-s-triazine rings, whereas the other bands in the 1250-1650 cm^{-1} region correspond to the typical stretching vibrations of aromatic C–N heterocycles. Furthermore, no peaks shift was observed in Co-g-C_3N_4 (pm), signifying that the molecular structure of g-C_3N_4 is not changed upon Co doping. The FTIR spectrum of Co-g-C_3N_4 (pm) displays two additional absorption bands at 571 and 667 cm^{-1}, arising from the stretching vibrations of Co-O bonds, which confirms the formation of spinel Co_3O_4 [18]. Two bands represent the vibrations of octahedrally and tetrahedrally coordinated Co^{3+} and Co^{2+} with oxygen in spinel lattice.

The N_2 adsorption and desorption isotherms were measured to characterize the specific surface area of g-C_3N_4 (pm) and Co-g-C_3N_4 (pm) (Fig. 4). The isotherms of both samples feature typical type-IV properties, which suggest the presence of porous (mesoporous and macroporous) structures. The hysteresis loop in the low pressure range ($0.5 < P/P_0 < 0.9$) is associated with the intra-aggregated pores. The calculated BET specific surface areas of pure and Co_3O_4 modified g-C_3N_4 (pm) was 5.8 and 11.7 m^2/g, respectively. Almost 2-fold enhanced specific area of the Co-g-C_3N_4(pm) after doping with cobalt could be attributed to the dispersion of fine Co_3O_4 nanoparticles in the C_3N_4 sheets thus preventing aggregation, which is also evident from the XRD result. A higher surface area of Co-g-C_3N_4 (pm) would favor the diffusion of reactants and provides

more active sites, leading to improved catalytic performance. For comparison, the surface area of the samples prepared from non-protonated melamine was 3.0 and 5.7 m^2/g, respectively.

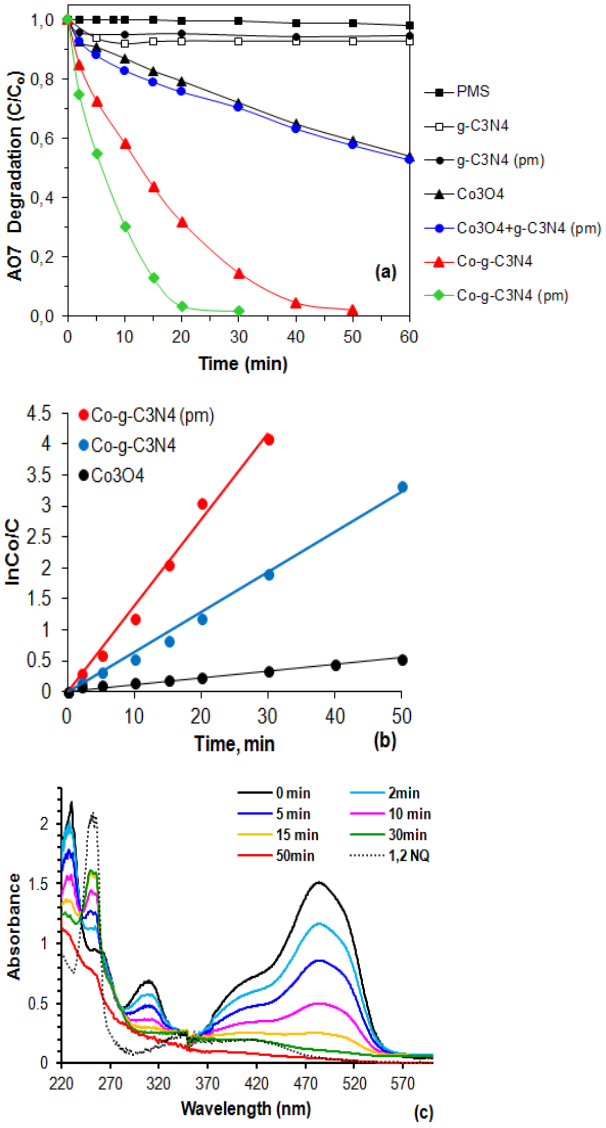

Figure 5. (a) Degradation profile of AO7 degradation in different systems, (b) degradation kinetics of AO7 by PMS activated by different catalysts, and (c) UV–vis spectral changes during AO7 degradation with Co-g-C_3N_4 (pm)/PMS system. Reaction conditions: 50 mg dm^{-3} AO7; 0.5 g dm^{-3} catalyst loading; PMS/AO7= 10/1; pH=3.0

The removal of AO7 based on chemical oxidation with PMS and catalytic degradation with different catalysts in the presence of PMS was evaluated, and the results are presented in Fig. 5a. The degradation of AO7 occurred very slowly in the presence of PMS alone without a catalyst. Less than 1 % AO7 removal was achieved after 1 h of reaction, implying that the chemical oxidation of dye occurs through a non-radical mechanism. Only 7% of the dye was removed after 60 min with pristine g-C_3N_4 and g-C_3N_4 (pm) coupled with PMS, pointing out that pure graphitic nitride possess negligible PMS activation ability at ambient conditions. A significant improvement of the catalytic performance of g-C_3N_4 was observed after modifying with Co_3O_4, indicating that PMS can be activated by the composite catalysts with the production of active radical species. The highest degradation rate was achieved in the Co-g-C_3N_4 (pm)/PMS system with complete dye removal after 30 min. When a composite obtained from non-protonated melamine was used as a catalyst, only 85% of AO7 was degraded for the same duration, but the dye could also be fully decolorized within 50 min. Evidently, synthesizing g-C_3N_4 by heating HNO_3 protonated melamine influences the PMS decomposition activity of the composite catalysts. The faster AO7 degradation kinetics assisted by Co-g-C_3N_4 (pm) catalyst may be related to its larger surface area, which can afford more active sites for catalysis than that of Co-g-C_3N_4. Further investigations on the effect of the protonation on the improved catalytic activity over the Co-g-C_3N_4 (pm) sample are underway. These results clearly indicated that the Co_3O_4 modified g-C_3N_4 is an active catalyst for remediation of dyes wastewater in the presence of PMS without light irradiation. Bare Co_3O_4 exhibited a much lower catalytic activity than Co-g-C_3N_4 hybrids with only about 41% AO7 removal efficiency after 50 min under similar conditions. Therefore, the enhanced catalytic performance of the composite catalysts could be attributed to the synergistic effect between the g-C_3N_4 and Co_3O_4 oxide. Decomposition of PMS to reactive radicals is based on the electron transfer from the catalyst to PMS. Besides basic surface functionalities, which are important for PMS activation, the delocalized d-electrons from the tri-s-triazine units of g-C_3N_4 can also contribute to electron transfer, so that PMS can decompose to radicals [12]. The crucial role of the close contact between the Co_3O_4 particles and the g-C_3N_4 was further confirmed by experiments using a physical mixture of Co_3O_4 and g-C_3N_4 (pm) as a catalyst for PMS activation. The results showed that the catalytic efficiency of the mechanical mixture is much lower than that of Co-g-C_3N_4 (pm) and close to that, exhibited by pristine Co_3O_4.

As shown in Fig. 5b, the AO7 degradation follows a pseudo-first-order kinetics. The rate constants are estimated to be 0.1391 min^{-1} (R^2= 0.991) and 0.0646 min^{-1} (R^2= 0.994) in the Co-g-C_3N_4(pm)/PMS and Co-g-C_3N_4/PMS systems, respectively. By contrast, corresponding to Co_3O_4/PMS system rate constant is 0.0109 min^{-1} (R^2= 0.987), which is about 12.4 and 5.9 times

lower than that exhibited by the composite catalysts, respectively. This strongly confirms the improved catalytic behavior of Co_3O_4 for activating PMS after dispersion on the g-C_3N_4 surface.

Representative UV–vis spectral changes observed during the Co-g-C_3N_4(pm)-mediated AO7 degradation are presented in Fig. 5c. As seen, the addition of catalyst and PMS into the dye solution caused a continuous decrease of the characteristic absorption bands in the visible region with time and finally disappeared after 20 min, indicating the destruction of the chromophore-containing azo-linkage. In parallel, the absorbance in the UV region is also reduced, due to the destruction of the conjugated π-system. Furthermore, concurrently with the decay in the visible region, a new band at 254 nm appeared at the very beginning of the reaction and then descended gradually in the late reaction stage. 1,2-naphthoquinone (1,2 NQ) was identified to contribute to the peak by comparing spectra of the reaction mixture and a standard solution containing 1,2 NQ.

Further kinetic studies were carried out using the most active Co-g-C_3N_4 (pm) catalyst to explore the effects of main operating parameters, namely catalyst dosage, PMS concentration, and initial solution pH on the AO7 degradation rate.

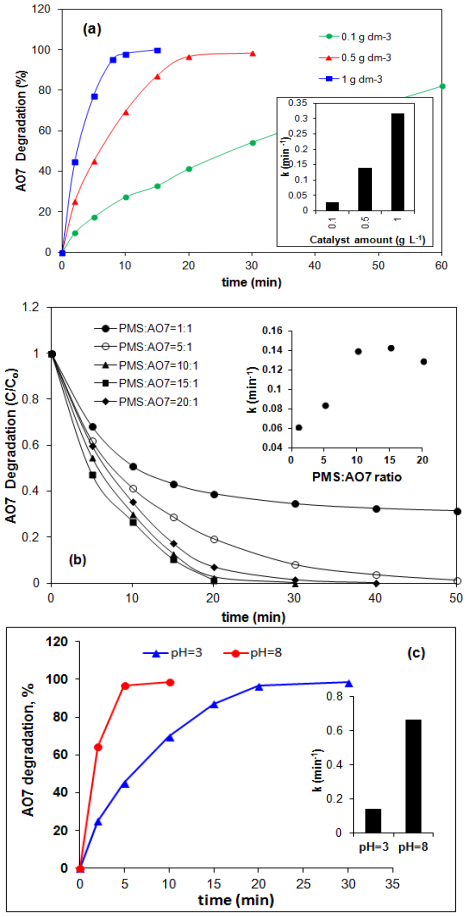

Figure 6. Effect of (a) catalyst dosage: PMS:AO7=1:1, pH=3; (b) PMS concentration: [catalyst]=0.5 g dm^{-3}, pH=3; (c) initial solution pH: [catalyst]=0.5 g dm^{-3}, PMS:AO7=1:1 on the AO7 catalytic oxidation over Co-*g*-C_3N_4 (pm).

As clearly shown in Fig. 6a, the increase in the catalyst amount from 0.1 g dm^{-3} to 1 g dm^{-3} resulted in an 11-fold increase in the degradation rate and accordingly, AO7 removal in 15 min was enhanced from about 33% to 100%. The observed trend can be attributed to the increased numbers of active sites for PMS activation and, hence, more radicals generated per unit time. These results also confirm the crucial role of the catalyst for the effective activation of oxidant, as well as indicate that the surface reaction is the rate limiting step.

The catalytic degradation of AO7 was also affected by the PMS dosage, as illustrated in Fig. 6b. As observed, both the AO7 degradation efficiency and the rate constant significantly increased first with increasing PMS:AO7 ratio from 1:1 to 10:1 and then only slightly changed at higher PMS dosages. At a molar ratio of 1:1 complete removal of AO7 was not achieved due to the lack of sufficient oxidant amount, whereas the ten-fold increase in PMS dosage led to more than 99% extent of dye decolorization for 30 min. As the concentration of PMS increases, more active radicals are produced and, hence, faster AO7 degradation occurs. However, the degradation rate becomes slower when the PMS:AO7 ratio is higher than 15:1, probably due to the self-quenching of sulfate radicals by PMS [19].

As shown in Fig. 6c, AO7 degradation in Co-g-C_3N_4 (pm)/PMS system is strongly affected by the initial pH of the solution. With increasing pH from 3 to 8 (adjusted with 1M NaOH), the rate constant increased from 0.1347 (R^2 = 0.997) to 0.6632 min^{-1}(R^2 = 0.984). Accordingly, at pH 8 almost 99% of AO7 is removed for only 5 min while 30 min are needed to achieve the same degradation efficiency in acidic medium. The observed pH dependence of the degradation rate is unexpected given the influence of pH on the surface charge of the catalyst and the fractions of different PMS species. As the isoelectric point of g-C_3N_4 obtained from melamine is reported to be about 5.0, below this value the surface of g-C_3N_4 was positively charged [20]. On the other hand, PMS exists in the form of HSO_5^- at acid-neutral conditions, while SO_5^{2-} are the dominant PMS species when pH was above 9.2 [21]. When pH is increased, the interaction between PMS and catalyst surface tends to decrease due to the electrostatic repulsion among them, thus less PMS could be activated and AO7 degradation rate could decrease.

However, a homogeneous activation of PMS by NaOH may take place in basic conditions. A mechanism of base-activation of PMS is proposed, according to which H_2O_2 is formed upon NaOH-catalyzed hydrolysis of PMS and subsequently, was decomposed to superoxide anion radicals [22]. Besides, PMS can decompose into sulfate and hydroxyl radicals in the presence of H_2O_2 [23]. Therefore, the observed higher AO7 degradation at pH 8 could be attributed to the simultaneous homogeneous activation of PMS by NaOH and its decomposition to radicals on the catalyst surface. At acidic pH, due to the formation of H-bond between H^+ and the O–O group of HSO_5^-, the PMS ions acquire a pseudo-positive charge, resulting in surface repulsion effect [24]. Moreover, under acidic condition the SRs could be scavenged by H^+, resulting in production of less reactive HSO_4^- [25]. Therefore, a lower degradation rate was observed at a lower pH.

Previous investigations have pointed out that sulfate radical ($SO_4^{\bullet -}$) and hydroxyl radical (•OH) can be the main reactive species generated by heterogeneous catalytic activation of PMS in the presence of Co-containing catalyst [21]. To confirm that AO7 degradation was a radical-involved process and to ascertain the dominant radical species generated in the Co-g-C_3N_4 (pm)/PMS system, quenching tests were conducted with the addition of ethanol and *tert*-butyl alcohol (TBA) as radical scavengers. Ethanol is considered as a universal scavenger for $SO_4^{\bullet -}$ and •OH, because it readily react with both radicals at high and comparable rate. For TBA, the scavenging rate constant is approximately 1000 times greater for •OH than that for $SO_4^{\bullet -}$, therefore it is considered as a particular scavenger for •OH [8, 21]. As shown in Fig. 7, the degradation efficiency of AO7 with the addition of TBA was slightly less than that without any scavenger, indicating that •OH radicals had a negligible contribution to the degradation of dye in Co-g-C_3N_4 (pm)/PMS system. However, when using the same amount of ethanol as a scavenger, a more significant inhibiting effect was observed and AO7 degradation decreased to 56% only, suggesting that sulfate radicals were the main reactive species in the Co-g-C_3N_4 (pm)/PMS system.

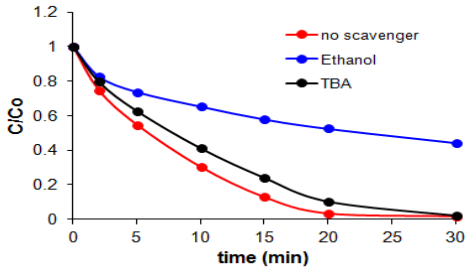

Figure 7. Inhibiting effect of scavengers (ethanol (TBA):PMS=1000:1 molar ratio) on AO7 degradation with Co-g-C_3N_4 (pm)/PMS system. Reaction conditions: as indicated in Fig. 5.

CONCLUSIONS

Co_3O_4 nanoparticles-modified g-C_3N_4 composites were prepared using a one-pot synthesis methodology and characterized by several techniques. The as-prepared materials were used as catalysts for PMS activation without light irradiation to produce sulfate radicals for degrading azo dye AO7. The Co-g-C_3N_4 (pm) composite prepared from protonated melamine showed the best performance in catalytic activation of PMS and was also proved more efficient than the bare Co_3O_4. The removal efficiency of AO7 with an initial concentration of 50 mg.dm^{-3} was greatly increased from 28% to 100% within 30 min with about 13 fold increase in the first order rate constant. Increasing catalyst dosage and pH was favorable to AO7 degradation, while high PMS concentration caused a slight decrease in the efficiency of the Co-g-C_3N_4 (pm)/PMS system. Radical pathway was proposed to contribute to AO7 degradation as sulfate radicals, being the dominating species, were generated by the catalyst/PMS interaction.

Acknowledgement: *Authors gratefully acknowledge financial support from by the University of Plovdiv Research Fund (Project NI HF-2017).*

REFERENCES

1. S. Yang, P. Wang, X. Yang, L. Shan, W. Zhang, X. Shao, R. Niu, *J. Hazard. Mater*., **179,** 552 (2010).
2. LW. Matzek, K.E. Carter, *Chemosphere*, **151**, 178 (2016).
3. W.-D. Oh, Z. Dong, G. Ronn, T.-T. Lim, *J. Hazard. Mater*., **325**, 71 (2017).
4. A. Ghauch, A.M. Tuqan, *Chem. Eng. J*., **183** 162 (2012).
5. M.M. Ahmed, S. Barbati, P. Doumenq, S. Chiron, *Chem. Eng. J*., **197**, 440 (2012).
6. Y. Feng, J. Liu, D. Wu, Z. Zhou, Y. Deng, T. Zhang, K. Shih, *Chem. Eng. J*., **280**, 514 (2015).
7. P. Hu, M. Long, *Appl. Catal. B*, **181,** 103 (2016).
8. G. Anipsitakis, D. Dionysiou, *Environ. Sci.Technol*., **37**, 4790 (2003).

9. J. Deng, S. Feng, K. Zhang, J. Li, H. Wang, T. Zhang, X. Ma**,** *Chem. Eng. J.*, **308,** 505 (2017).
10. C. Wang, P. Shi, X. Cai, Q. Xu, X. Zhou, X. Zhou, D. Yang, J. Fan, Y. Min, H. Ge, W.Yao, *J. Phys. Chem. C*, **120,** 336 (2016).
11. H. Yang, K. Lv, J. Zhu, Q. Li, D. Tang, W. Ho, M. Li, S.A.C. Carabineiro, *Appl. Surf. Sci.*, **401**, 333 (2017).
12. C. Wang, J. Kang, H. Sun, H.M. Ang, M.O. Tadé, S. Wang, *Carbon*, **102**, 279 (2016).
13. H. Liu, P. Sun, M. Feng, H. Liu, S. Yang, L. Wang, Z. Wang, *Appl. Catal. B*, **187**, 1 (2016).
14. Y. Zheng, Y. Jiao, Y. Zhu, Q. Cai, A. Vasileff , L. H. Li, Y. Han, Y. Chen, S-Z. Qiao, *J. Am. Chem. Soc.*, **139**, 3336 (2017).
15. F. Ghanbari; M. Moradi, *Chem. Eng. J.*, **310**, 41 (2017).
16. J. Li, J. F. P. Ye, D. Wu, M. Wang, X. Li, A. Xu, *J. Photoch. Photobio.* A, **342**, 85 (2017).
17. S. Hu, X. Chen, Q. Li, F. Li, Z. Fan, H. Wang,Y. Wang, B. Zheng, G. Wu, *Appl. Catal. B-Environ.*, **201**, 58 (2017).
18. Z.S. Wu, W.C. Ren, L. Wen, L. Gao, J. Zhao, Z. Chen, G. Zhou, F. Li, H.-M. Cheng, *ACS Nano*, **4**, 3187 (2010).
19. M. Antoniou, A. de la Cruz, D. Dionysiou, *Appl. Catal., B*, **96**, 290 (2010).
20. B. Zhu, P. Xia, W. Ho, J. Yu, *Appl. Surf. Sci.*, **344,** 188 (2015).
21. J. Deng, C. Ya, Y. Ge, Y. Cheng, Y. Chen, M. Xu, H. Wang, *RSC Adv.*, **8**, 2338 (2018).
22. R. Xiao, Z. Luo, Z. Weis, S. Luo, R. Spinney, *Curr. Opin. Chem. Eng.*, **19**, 51 (2018).
23. J. Zhao, Y. Zhang, X. Quan, S. Chen, *Sep. Purif. Technol.*, **71**, 302 (2010).
24. Y. Guan, J. Ma, X. Li, J. Fang, L. Chen, *Environ. Sci. Technol.*, **45**, 9308 (2011).
25. Y.-H. Huang, Y.-F. Huang, C.-I. Huang, C.-Y. Chen, *J. Hazard. Mater.*, **170**, 1110 (2009).